

# Gradient Boundary Histograms for Action Recognition

Feng Shi, Robert Laganière and Emil Petriu  
School of Electrical Engineering and Computer Science  
University of Ottawa, Ottawa, On, Canada  
{fshi098, laganier, petriu}@eeecs.uottawa.ca

## Abstract

*This paper introduces a high efficient local spatio-temporal descriptor, called gradient boundary histograms (GBH). The proposed GBH descriptor is built on simple spatio-temporal gradients, which are fast to compute. We demonstrate that it can better represent local structure and motion than other gradient-based descriptors, and significantly outperforms them on large realistic datasets. A comprehensive evaluation shows that the recognition accuracy is preserved while the spatial resolution is greatly reduced, which yields both high efficiency and low memory usage.*

## 1. Introduction

Recent studies in human action recognition have achieved remarkable performance. Over the years, the progress has shown almost perfect results on atomic actions captured under controlled settings. As a result, the research community now focuses on realistic datasets with relatively large number of classes, and very good results are reported [14, 26, 22]. However, much effort has been invested in improving the recognition accuracy with less consideration in efficiency. For example, the state-of-the-art approach [22] combines both SURF feature matches and dense matches from optical flows to estimate the homography for camera motion compensation. To further improve the robustness, it also uses a sophisticated human detector as well as human tracking to remove matches from the foreground human regions. All these techniques add more complexity to the already high cost trajectories-based method, which is built on dense optical flow.

The low-level local spatio-temporal features and bag-of-features(BoF) [14, 15, 21] representation or alternative Fisher vector encoding [22, 11] can achieve good performance for action recognition on realistic datasets. A key factor for high performance is the local descriptors, which should include both local structure and motion information. Among all descriptors, MBH outperforms other descriptors by encoding motion boundary and suppressing camera mo-

tion. However, to build up MBH, dense optical flows are computed for consecutive frames. Dense optical flow is expensive to compute considering the large amount of video data to be processed. In addition, it includes two descriptors, MBHx and MBHy, which add to the dimensionality and complexity for codeword quantization. Therefore, it is desirable to develop high efficient descriptors, especially for real-time applications, such as intelligent surveillance system with multiple cameras, human-machine interaction and video games.

Gradient-based descriptors, on the other hand, are fast to compute. However, they often show suboptimal performance and high feature dimensionality. Built on oriented gradient, the HOG descriptor was originally introduced by Dalal and Triggs in [2] for human detection. It only contains local structure information and shows low recognition accuracy on action recognition due to lack of motion information. For better performance, it is often combined with HOF descriptor [9], which requires the computation of dense optical flow.

Kläser [7] extended HOG descriptor from 2D image to spatio-temporal HOG3D descriptor with 3D oriented gradients. The spatio-temporal gradients ( $\frac{\partial I}{\partial x}$ ,  $\frac{\partial I}{\partial y}$ ,  $\frac{\partial I}{\partial t}$ ) are computed for each pixel over the video, and saved in three integral videos. Three gradient components of a ST patch can be computed efficiently from the integral videos. The mean 3D gradient vector from a local cell is quantized using a regular polyhedron. The 3D histograms of oriented gradients for the 3D patch are formed by concatenating gradient histograms of all cells. Although it is very efficient to compute gradients, the quantization with polyhedron for each sub-blocks is expensive considering the large number of patches sampled. The 3D quantization also results in high feature dimension. In addition, using regular polyhedron with congruent faces to quantize the ST gradients may not be an optimal option because the units of spatial gradients and temporal gradients in a video are different and should not be treated interchangeably.

Scovanner *et al.* [13] extended 2D SIFT descriptor [10] to represent spatio-temporal patches, called 3D SIFT. Once

gradient magnitude and orientation computed in 3D, each pixel has two values  $(\theta, \phi)$  which represent the direction of the gradient in three dimensions. For orientation quantization, the gradients in spherical coordinates  $(\theta, \phi)$  are divided into equally sized bins, which are represented by an  $8 \times 4$  histogram. Such representation leads to singularity problems as bins get progressively smaller at the poles. Similar to HOG3D, it also has increased dimensionality, and treats spatial and temporal gradients as similar quantities.

In this paper, we focus on developing an efficient method for action recognition on realistic videos. Our method is based on pure spatio-temporal gradients. However, our objectives are both to improve the performance and to avoid high dimensionality of common 3D gradient-based descriptors, such as HOG3D and 3D SIFT. In addition, we also aim at reducing the memory usage. To this end, we made following main contributions:

- We propose a new spatio-temporal descriptor, called GBH, which significantly outperforms other gradient-based descriptors both in performance and speed.
- In an in-depth experimental evaluation, we demonstrate that the recognition accuracy is preserved while the spatial resolution is greatly reduced, which yields to both high efficiency and low memory usage.
- We rigorously show that the proposed descriptor and its Fisher vector representation can achieve real-time activity analysis with potential application in mobile computation.
- We experimentally show that the GBH descriptor can improve recognition performance significantly when combined with HOF or MBH descriptor.

The paper is organized as follows: The next section introduces the proposed GBH descriptor. Section 3 details the methods we use. Section 4 summarizes the evaluation methodology as well as the datasets. In section 5, we present some experimental results and analysis. we also provide the comparison of our methods with the state-of-the-art. The paper is completed with a brief conclusion.

## 2. Gradient boundary histograms (GBH) descriptor

In this paper, we propose a new local spatio-temporal descriptor. Our object is to avoid the expensive dense optical flow computation. We also intend to encode both local static appearance and motion information. However, we want to avoid using three gradient components as 3D SIFT and HOG3D descriptor which lead to high dimensionality and relatively expensive quantization cost. Instead, we

adopt compact HOG-like descriptor with two gradient components.

For each frame in a video, we first compute image gradients using simple 1-D [-1,0,1] Sobel masks on both  $x$  and  $y$  directions. Then, we apply a [-1, 1] temporal filter over two consecutive gradient images. Thus, for each pixel, we have:

$$I_{t,x} = \frac{\partial}{\partial t} \left( \frac{\partial I}{\partial x} \right), \quad I_{t,y} = \frac{\partial}{\partial t} \left( \frac{\partial I}{\partial y} \right) \quad (1)$$

Now the gradient magnitude and orientation for each pixel are defined as follows:

$$r(x, y) = \sqrt{I_{t,x}^2 + I_{t,y}^2}, \quad \theta(x, y) = \arctan\left(\frac{I_{t,y}}{I_{t,x}}\right) \quad (2)$$

Our new descriptor uses a histogram of orientation method, voting with  $\theta$  and  $r$  as in SIFT and HOG descriptors. However, instead of using image gradients, we use time-derivatives of image gradients, which emphasize moving edge boundaries. We call this descriptor gradient boundary histograms (GBH). Figure 1 illustrates the comparison of image gradients and gradient boundaries. We have two important observations here. First, the subtraction of two consecutive image gradients results in the removal of the backgrounds of the video sequences. The two gradient images in the centre show a lot of background noise, while the gradient boundary images on the right show clear human shapes with far less background noise. More important, gradient boundaries encode the moving human shapes. As demonstrated by the red bounding boxes in the figure, the double edges at various distances are proportional to the moving speed of the human body parts. For example, the distance between the leg double edges is larger than the head double edges, because the leg moves faster than the head of the other person in the upper right image.

It seems that the simple gradient subtraction works well only when the camera and background are largely static. However, our in-depth experimental evaluations show that it also achieves good performance on realistic HMDB51 dataset, which contains a lot of camera motions and dynamic backgrounds. One possible explanation may be that the changes of the human gradient boundary (as shown in Figure 1) reflect the speed of the moving body parts. Because the camera motion for two consecutive frames is often constant, the subtraction of two consecutive gradient images results in a constant gradient offset. Therefore, the computed human gradient boundaries include the absolute gradient displacements of human moving body plus a constant gradient displacement. Such constant gradient displacement from the camera motion has little performance impact.

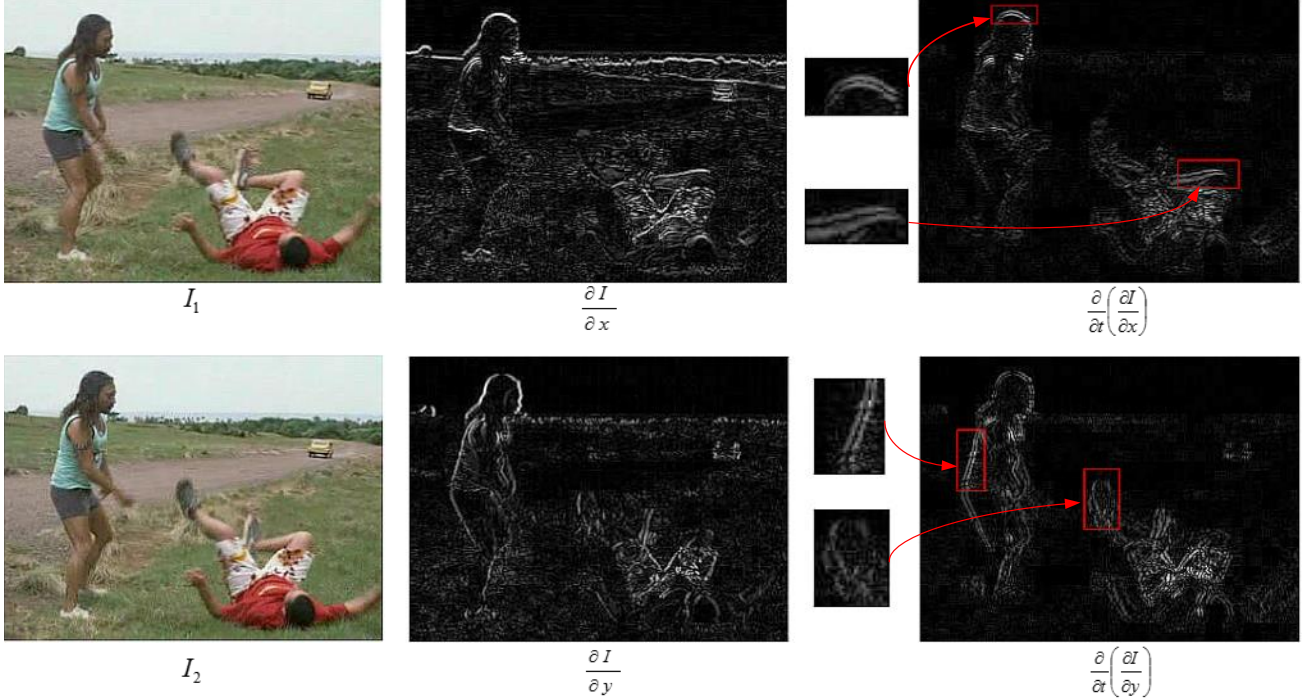


Figure 1. Illustration of gradients and gradient boundaries for a “fall floor” action. Compared to image gradients, gradient boundaries have less background noise. More important, gradient boundaries encode motion information. The areas inside red bounding boxes show the double edges at distances proportional to the speed of the moving body parts.

### 3. Video representation

To demonstrate the performance of the proposed GBH descriptor, we apply an efficient random sampling scheme to extract the features, and use the state-of-the-art local part model (LPM) [15] to represent them. We finally use improved fisher vector [12] to encode features, followed by a linear SVM for classification.

#### 3.1. Review of LPM algorithm

Local part model was introduced by Shi *et al.* in [16]. Their original purpose was to address the orderless issue of the bag-of-features representation by introducing overlapping local “parts” in the same spirit as bi-gram (n-Grams) [19]. In addition to having the overlapping local part patches, the method also includes a coarse primitive level “root” patch which encodes local global information. To improve the efficiency of LPM computation, two integral videos are computed, one for the root at half resolution, and another one for the parts at full resolution. The descriptor of a 3D patch can then be computed very efficiently through 7 additions multiplied by the total number of root and parts.

Later, Shi *et al.* [15] improved the efficiency by combining random sampling method with local part model. Random sampling does not require feature detection, which greatly improves processing speed. In this work, the root

and 8 parts are processed as two separate channels. For each channel, a standard Fisher vector encoding is applied. The resulting Fisher vectors from root and parts are concatenated into one histogram for SVM classification.

The main challenge of applying FV encoding on the features of LPM is the high dimensionality. The part channel in LPM contains a group of overlapping patches, and their histograms are concatenated into a high dimensional vector. Therefore, as discussed in next section, we reduce the descriptor dimensionality by using Principal Component Analysis (PCA) on the purpose of better fitting FV encoding. In our experiments, the dimensions of root descriptor and part descriptor are reduced by 1/2 and 1/8, respectively.

#### 3.2. Fisher vector encoding

Recent studies [22, 11, 18] show that Fisher vector [5] can improve performance over standard bag-of-features methods on action recognition. FV extends the bag-of-features by encoding high-order statistics between the descriptors and a Gaussian Mixture Model. Since more information is encoded per visual word, fewer visual words are required than BoF, which makes FV more efficient to compute.

As indicated in [5], it is favourable to apply PCA dimensionality reduction on feature vectors before FV encoding.

Moreover, for a  $D$  dimension descriptor, the FV signature with  $K$  words has an increased dimension of  $2DK$ . In the case of local part model, the concatenated histograms of part patches result in 8 times the dimension of the used descriptor. Therefore we apply PCA on the computed LPM features. Our experimental evaluation shows that the feature dimensions can be reduced by 7/8 while preserving high accuracy.

## 4. Experimental setup

In this section, we introduce implementation details of our evaluation methodology. We will also present the datasets and experimental parameters.

### 4.1. Evaluation methodology

As discussed in Section 3, we use random sampling for feature extraction and local part model to represent the features. We strictly follow the experimental settings as those in [15]. However, we use Fisher vector encoding instead of bag-of-features.

We randomly choose 10000 features for each video with maximal video length of 160 frames. For those clips with more than 160 frames, we simply divide them into several segments, and sample features at same rate for each of them.

The sampled 3D patches are represented by GBH descriptor. Under the LPM representation, each feature includes a root patch and a group of part patches (8 in our experiments). Let  $D_0$  be the feature dimension of the GBH descriptor. One LPM feature has two channels, with 1 root at dimension  $d_r = D_0$  and 8 parts of dimension  $d_p = 8 \times D_0$ .

For colour images, we simply choose the channel with largest gradient values, which improves the accuracy by 0.2-0.5%.

For Fisher vector encoding, we use improved fisher vector [12] by applying the signed square-rooting followed by  $L_2$  normalization, which significantly improves the performance when combined with a linear classifier. We set the number of visual words to  $K = 128$  and randomly sample 150,000 features from the training set to estimate the GMM and learn PCA projection matrix. For Fisher vector encoding, we first apply PCA to reduce root vectors to  $d'_r = \frac{1}{2}d_r = \frac{1}{2}D_0$  and part vectors to  $d'_p = \frac{1}{8}d_p = D_0$ . Each video is, then, represented by a  $2d'_rK + 2d'_pK = 3D_0K$  dimensional Fisher vector.

The resulting Fisher vectors are fed into a linear SVM implemented by LIBSVM [1] with  $C = 32.5$ . For multi-class SVM, we use one-against-rest approach. To combine root and part channels of LPM representation, we simply concatenate the computed FVs from the respective channels. The same strategy is used to combine multiple channels from different descriptors.

## 4.2. Datasets

To demonstrate the performance and efficiency of the proposed descriptor, we evaluate our method on two large-scale realistic action benchmarks, the UCF101 [17] and the HMDB51 [8] datasets.

The **UCF101** dataset [17] is by far the largest human action dataset. It has 101 classes and 13320 realistic video clips extracted from YouTube. All clips are encoded at a resolution of  $320 \times 240$  and at a frame rate of 25 FPS. The clips of one action class are divided into 25 groups. The dataset is very large and relatively challenging. We report average accuracy over three distinct training and testing splits as proposed in [17]. For split 1, split 2 and split 3, clips from groups 1-7, groups 8-14 and groups 15-21 are selected respectively as testing samples, and the rest for training.

The **HMDB51** dataset [8] contains 51 action categories, with a total of 6,766 video clips extracted from various sources, such as Movies, the Prelinger archive, Internet, Youtube and Google videos. It is perhaps the most challenging dataset with realistic settings. The videos have different aspect ratio, but with a fixed height of 240 pixels. The clips have various video quality, and the minimum quality standard is at 60 pixels in height for the main actor. We use the original non-stabilized videos with the same three train-test splits [8], and report the average accuracy over the three splits in all experiments.

### 4.3. Parameters

In this section, we present our parameter settings, which determine the features' dimension. We test and compare our GBH descriptor with other descriptors. However, we use the simplified HOG3D, HOG and MBH descriptors with reduced dimensionality, mainly by controlling the number of cells per ST patch.

*Notation:* we define the sampling grid at half the spatial resolution of the processed video. The root patches are randomly chosen from this half size video, and we will refer to it as "root video". The part patches are sampled from the processed video at full spatial resolution, which is referred to as "part video" or "processed video", interchangeably. We also use "original video" to represent the original spatial resolution of the clips from the datasets.

**Random sampling.** In order to provide comparable results, we strictly follow the sampling parameter settings as those in [15]. We first define a very dense sampling grid over the root video. A 3D video patch centred at  $(x, y, t)$  is sampled with a patch size determined by the multi-scale factor  $(\sigma, \tau)$ . The consecutive scales are computed by multiplying  $\sigma$  and  $\tau$  by a factor of  $\sqrt{2}$ . In our experiments, we set minimal temporal size to 14 frames, and choose the optimal minimal spatial size based on the descriptors and the

Smoothing	HMDB51			UCF101		
	HOG	HOG3D	GBH	HOG	HOG3D	GBH
Yes	29.4%±0.6	37.8%±0.6	44.4%±0.3	60.6%±0.2	64.5%±0.9	74.6%±0.3
No	30.0%±0.3	38.2%±0.3	40.2%±0.7	61.2%±0.5	64.7%±0.4	73.0%±0.6

Table 1. The performance impact of Gaussian smoothing on different descriptors. The experiments are performed on the video at original resolution.

Resolution	HMDB51			UCF101		
	HOG	HOG3D	GBH	HOG	HOG3D	GBH
(avg.)364 x 240	30.0%±0.3	38.2%±0.3	44.4%±0.3	61.2%±0.5	64.7%±0.4	74.6%±0.3
182 x 120	27.5%±0.5	36.5%±0.2	44.7%±0.3	55.4%±0.4	63.6%±0.2	74.2%±0.4
91 x 60	23.7%±0.4	33.0%±0.7	45.3%±2.4	50.5%±0.4	56.6%±0.7	73.6%±0.9

Table 2. The performance comparison of three gradient-based descriptors at different spatial resolutions.

size of the processed video. The sampling step size is determined by multiplying patch size by a factor of 0.2. With a total of 8 spatial scales and 2 temporal scales, we sample a video 16 times.

We randomly sample 10000 root patches from the root video. For each root patch, we sample 8 ( $2 \times 2 \times 2$ ) overlapping part patches from the part video. The histograms of 1 root patch and 8 part patches are treated as two separate channels.

**GBH, HOF, MBH<sub>x</sub> and MBH<sub>y</sub>.** Each patch is subdivided into a grid of  $2 \times 2 \times 2$  cells, with no sub-block division. 8 bins are used for quantization, which leads to a feature dimension of 64. Thus, a LPM feature has a root channel of dimension 64 and a part channel of dimension 512.

We evaluate GBH descriptor on the processed video with different spatial resolutions. When the processed video has same size as original video, the initial patch size is  $28 \times 28 \times 14$ . We use minimal patch size of  $20 \times 20 \times 14$  and  $10 \times 10 \times 14$ , respectively, for the part video size at half and one quarter.

**HOG.** For HOG, we use same parameters as GBH in most cases. However, for original video size, the optimal minimal patch size is  $24 \times 24 \times 14$ , and each patch is subdivided into a grid of  $2 \times 2 \times 2$  cells, with  $2 \times 2 \times 2$  sub-block divisions. With 8 bins quantization, It has same feature dimension as GBH.

**HOG3D.** The HOG3D parameters are: number of histogram cells  $M = 2$ ,  $N = 2$ ; number of sub-blocks  $1 \times 1 \times 3$ ; and polyhedron type dodecahedron(12) with full orientation. The optimal minimal patch size is  $24 \times 24 \times 14$  for original video size. With one HOG3D descriptor at dimension of 96 ( $2 \times 2 \times 2 \times 12$ ), our local part model feature has a dimension of 96 for the root channel and 768 for the part channel.

## 5. Experimental results

In this section, we evaluate performance of the proposed GBH descriptor for action classification on two realistic

datasets. Due to the random sampling, we repeat the experiments 3 times, and report mean accuracy and standard deviation over 3 runs.

### 5.1. Influence of Gaussian smoothing

We first evaluate the impact of the Gaussian smoothing. The results are show in Table 1. All the experiments are performed on original video at full resolution. If smoothing is “Yes”, a Gaussian filter is applied on all frames before computing the gradients.

For HOG and HOG3D descriptors, we observe slight performance drops on all cases when applying Gaussian filter before computing gradients. Similar performance drop is reported on HOG on human detection [2] with smoothing. The performance of GBH, on the other hand, increases significantly by pre-smoothing, with 4.2% on HMDB51 and 1.6% on UCF101. Such a performance increase may be explained by the fact that the second order derivatives are more sensitive to noise. In addition, applying Gaussian smoothing before gradient subtraction results in the suppression of certain background gradients, such as tree leaves and grass textures (as shown in Figure 1). Such background textures are often a huge challenge to optical flow estimation.

### 5.2. Evaluation of GBH descriptor

Table 2 shows the performance comparison of three gradient-based descriptors in different spatial resolutions. For HOG and HOG3D descriptors, the performance is consistently and significantly decreased for both HMDB51 and UCF101 when the spatial resolution is reduced. Such results are consistent with observations in [23] on Hollywood2 dataset. As resolution is reduced, the background gradients interfere with the gradients associated with human subjects.

For GBH descriptor, one very important observation is that the accuracy is preserved on HMDB51 and with little (1%) loss on UCF101 when the spatial resolution is reduced

Dataset	GBH	HOG	HOG3D	HOF	MBH	HOG+HOF	HOF+GBH	MBH+GBH
HMDB51	44.7%	30.0%	38.2%	39.9%	54.7%	45.6%	51.3%	58.8%
UCF101	74.2%	61.2%	64.7%	65.9%	81.0%	75.4%	78.0%	84.0%

Table 3. Performance comparison of the proposed GBH descriptor and other local descriptors.

by a factor of  $\lambda = 4$ . This leads to huge benefits in efficiency considering that the sub-sampling in resolution by  $\lambda$  results in a reduction by a factor of  $\lambda^2$  on both number of processed pixels and memory usage. Kläser *et al.* [7] observed, in a HOG3D approach, that using integral video can result in a reduction factor of 21 in memory usage when compare to spatio-temporal “pyramids”. Our method uses even less memory when processing video at low resolution.

When processing video at a very low resolution, we observe a relatively high standard deviation on performance for both HMDB51 (2.4) and UCF101 (0.9). This is probably due to the fact that the sampling is performed on the very low resolution video. At such low resolution, a sampled ST patch could have large differences even for a one pixel displacement. At this point, it is unclear why the GBH descriptor performs better at very low spatial resolution (91 x 60) on HMDB51 than on UCF101. Our hypothesis is that high sampling density on clips with fewer frames may include more information, which could provide bias benefits for the short clips of HMDB51. Moreover, the HMDB51 has a quality standard of a minimum of 60 pixels in height for the main actor, which may improve the robustness when the spatial resolution is greatly reduced.

### 5.3. Comparison of GBH and other descriptors

We perform a number of experiments to evaluate our proposed GBH descriptor. Table 3 shows the performance comparison of the GBH descriptor and other local descriptors. The evaluation is performed under a common experimental setup. The HOG and HOG3D descriptors are computed at full resolution, and other descriptors are computed at half the resolution. We use the default parameters as in Section 4.3, and randomly choose 10K features (that is 10K root patches + 80K part patches) from each clip with up to 160 frames. The dense optical flow for HOF and MBH descriptors is computed using efficient Farneback’s approach [3].

The GBH descriptor gives surprisingly good results by itself, with 44.7% on HMDB51 and 74.2% on UCF101. It outperforms HOG, HOG3D and HOF descriptors on both datasets. However, the MBH descriptor outperforms all other descriptors by a large margin. When combined with flow-based HOF or MBH descriptor, we observe significant performance improvements.

Method		HMDB51	UCF101
HMDB51 [8]		23.2%	–
UCF101 [17]		–	43.9%
Efficient OF [6]		46.7%*	–
DCS [4]		52.1%*	–
FV coding[11]		54.8%*	–
Trajectories [22]		57.2%*	85.9%*
Ours	GBH	44.7%±0.3	74.2%±0.4
	MBH <sup>1</sup>	54.7%±0.2	81.0%±0.2
	MBH <sup>2</sup>	58.9%±0.3	84.7%±0.1
	GBH + MBH <sup>1</sup>	58.8%±0.2*	84.0%±0.2*
	GBH + MBH <sup>2</sup>	<b>62.0%±0.2*</b>	<b>86.6%±0.2*</b>

Table 4. Comparison of average accuracy on HMDB51 and UCF101 with state-of-the-art methods. Those marked with \* are results with multiple descriptors. The MBH<sup>1</sup> is based on the Farneback’s optical flow method [3], and MBH<sup>2</sup> uses duality-based TV.L1 approach [25].

### 5.4. Comparison to state-of-the-art

Table 4 shows the comparison of our method with the state-of-the-art. We set the part video at the half the spatial resolution of original video, and use the parameters listed in Section 4.3. Most state-of-the-art methods use multiple descriptors and apply some feature encoding algorithms to improve the performance. For example, Jain *et al.* [4] combine five compensated descriptors and apply VLAD representation. Wang and Schmid [22] use four descriptors and Fisher Vector encoding. They also improve the performance with human detection and extensive camera motion compensation.

On **HMDB51**, our method achieves 62.0% when combining GBH with MBH descriptors, which outperforms the state-of-the-art result (57.2% [22]) by 5%. With MBH computed from efficient Farneback optical flow method, we obtain 58.8% on the two descriptors (MBH+GBH), which also exceeds state-of-the-art results. Note that our results are obtained from two descriptors combined with Fisher vector. Since we have both root and part channels, we set  $K = 128$  for FV encoding. Thus, our resulting FV features have same dimensionality as those in [22], which uses  $K = 256$ . In the case of  $K = 256$ , we achieve **63.2%**.

On **UCF101**, we report 86.6% with two descriptors. It slightly outperform the state-of-the-art result [22] (85.9%), which is obtained with four descriptors and Fisher Vector encoding as well as extensive camera motion estimation.

Dataset	Resolution	Speed (frames per second)				Mean accuracy
		Integral video	Sampling	FV encoding	Total fps	
HMDB51	364 x 240	120.5	249.5	151.7	52.8	44.4%
	182 x 120	302.9	261.4	150.5	72.5	44.7%
	91 x 60	437.5	294.4	156.8	82.7	45.3%
UCF101	320 x 240	132.8	356.7	220.2	67.2	74.6%
	160 x 120	362.9	384.7	223.7	101.8	74.2%
	80 x 60	596.2	422.2	228.5	118.5	73.6%

Table 5. Average computation speed with single core at different stages in frames per second.  $K = 128$  codewords per channel is used for FV encoding, and 10K features are sampled in the experiment. The dimensionality reduction process is included in FV encoding. Note that the classification stage is not included.

Sampling #	Resolution	Speed (frames per second)				Accuracy
		Integral video	Sampling	FV encoding	Total fps	
4K	182 x 120	52.7	267.6	89.3	29.0	43.3%
10K	182 x 120	52.9	108.4	37.5	18.3	44.7%

Table 6. Average computation speed on a Toshiba Netbook with an AMD-E350 cpu and 2GB memory. The experiments are performed on HMDB51 dataset.  $K = 128$  codewords per channel is used for FV encoding. 4K and 10K features are sampled in two different experiments. The dimensionality reduction process is included in the FV encoding.

## 5.5. Computational efficiency

We perform a number of experiments to evaluate the efficiency of GBH descriptor. We use VLFeat library [20] for Fisher vector encoding. The runtime is estimated on an Intel i7-3770K PC with 8GB memory. The prototype is implemented in C++. In order to avoid built-in multi-core processing of VLFeat library and OpenCV library, we set only one core active @ 3.5Ghz in Bios, and disable both Hyper-threading and Turbo-boost. For all experiments,  $K = 128$  visual words per channel are used for Fisher vector encoding.

Table 5 compares the computational speed under different spatial resolutions. For all cases, GBH achieves high processing speed, reported in frames per second. Using low resolution results in an impressive total fps at only little performance cost. There is little speed difference between HMDB51 and UCF101, mainly because on average we sample 10K features per 95 frames on HMDB51, but per 160 frames on UCF101.

Table 6 lists average computation speed on an AMD-E350 CPU, which also shows a high processing frame rate. This proves the high efficiency of GBH descriptor, and demonstrates its potential for real-time applications as well as mobile recognition.

## 6. Discussion

The GBH descriptor shows good performance with high efficiency. One possible application is action recognition for surveillance system with multiple static cameras. The efficient action detection, which involves the evaluation of multiple detection windows, can also benefit from the approach. GBH could also be used to improve the HOG

performance on human detection from the video. To further improve performance, we can also explore deeper part hierarchies (*i.e.* parts with parts). Since the GBH performance is preserved when using low resolution, we could add another layer of parts on full resolution videos. Our preliminary experiments on GBH descriptor with FV show that adding another level of parts improves the performance from 44.7% to 46.0% on HMDB51, and from 74.2% to 76.1% on UCF101.

We have shown that GBH can be combined with flow-based HOF or MBH descriptors to improve its performance. The dense optical flow on which HOF and MBH rely is relatively expensive to compute. However, this optical flow can be estimated very efficiently in compressed domain [24]. Recent progress in hardware and network technologies leads to motion-encoded videos, such as those obtained from internet protocol (IP) cameras in security and surveillance video systems. A recent study [6] also demonstrates the efficiency of extracting optical flow in compressed video, and achieves results similar to our GBH descriptor (45.4% on HMDB51 with MBH). Nevertheless, such approaches could be combined with our GBH descriptor to achieve state-of-the-art performance with high efficiency.

We have demonstrated that GBH outperforms other gradient-based HOG, HOG3D descriptors and flow-based HOF descriptors. Also, the GBH descriptor works well not only on static videos but also on non-static-camera videos, such as HMDB51. The performance may be further improved by explicitly estimating camera motion [22] or combining it with efficient MBH descriptor [6]. The main purpose of the GBH descriptor is to improve efficiency as well as to provide rich motion information. An efficient descrip-

tor with high performance can find many different applications in video analysis.

The main challenge in using FV is the resulting high dimensionality, which is expensive in classification stage even by using linear SVM. In comparison with BoF (often with 4K words), the FV representation is not much as a “Compact Feature Set” as the claim made in [11]. The original FV approach [5], however, reduces the high dimensional FV into a compact low dimensional vector and observes improved performance on image search. Considering its high dimensionality, it is desirable to improve the performance of individual descriptor, and combine fewer descriptors for high accuracy.

## 7. Conclusions

This paper introduces a spatio-temporal descriptor for action recognition. The proposed descriptor is based on ST gradients, and outperforms other gradient-based descriptors. We demonstrate its benefits in combination with Fisher vector representation. We experimentally show that the performance is preserved even when the spatial resolution is greatly reduced. Compared with existing methods, a major strength of our method is its very high computational efficiency, with potential for mobile applications.

## References

- [1] C.-C. Chang and C.-J. Lin. Libsvm: a library for support vector machines. *ACM Transactions on Intelligent Systems and Technology*, 2(3):27, 2011. 4
- [2] N. Dalal and B. Triggs. Histograms of oriented gradients for human detection. In *CVPR*, volume 1, pages 886–893. IEEE, 2005. 1, 5
- [3] G. Farnebäck. Two-frame motion estimation based on polynomial expansion. In *Proceedings of the 13th Scandinavian Conference on Image Analysis*, pages 363–370, 2003. 6
- [4] M. Jain, H. Jégou, and P. Boutheymy. Better exploiting motion for better action recognition. In *CVPR*, 2013. 6
- [5] H. Jégou, F. Perronnin, M. Douze, J. Sánchez, P. Pérez, and C. Schmid. Aggregating local image descriptors into compact codes. *Pattern Analysis and Machine Intelligence, IEEE Transactions on*, 34(9):1704–1716, 2012. 3, 8
- [6] V. Kantorov and I. Laptev. Efficient feature extraction, encoding and classification for action recognition. In *Computer Vision and Pattern Recognition, CVPR 2014*. IEEE, 2014. 6, 7
- [7] A. Kläser, M. Marszałek, and C. Schmid. A spatio-temporal descriptor based on 3d-gradients. In *BMVC*, pages 995–1004, 2008. 1, 6
- [8] H. Kuehne, H. Jhuang, E. Garrote, T. Poggio, and T. Serre. Hmdb: A large video database for human motion recognition. In *ICCV*, pages 2556–2563, 2011. 4, 6
- [9] I. Laptev, M. Marszałek, C. Schmid, and B. Rozenfeld. Learning realistic human actions from movies. In *CVPR*, 2008. 1
- [10] D. G. Lowe. Distinctive image features from scale-invariant keypoints. *IJCV*, pages 91–111, 2003. 1
- [11] D. Oneață, J. Verbeek, and C. Schmid. Action and event recognition with fisher vectors on a compact feature set. In *IEEE International Conference on Computer Vision (ICCV)*, 2013. 1, 3, 6, 8
- [12] F. Perronnin, J. Sánchez, and T. Mensink. Improving the fisher kernel for large-scale image classification. In *ECCV*, 2010. 3, 4
- [13] P. Scovanner, S. Ali, and M. Shah. A 3-dimensional sift descriptor and its application to action recognition. In *Proceedings of the 15th international conference on Multimedia*, pages 357–360. ACM, 2007. 1
- [14] F. Shi, R. Laganieri, E. Petriu, and H. Zhen. Lpm for fast action recognition with large number of classes. In *THUMOS: ICCV Workshop on Action Recognition with a Large Number of Classes*, 2013. 1
- [15] F. Shi, E. Petriu, and R. Laganieri. Sampling strategies for real-time action recognition. In *Proc. IEEE Conf. Computer Vision Pattern Recognition. IEEE*, 2013. 1, 3, 4
- [16] F. Shi, E. M. Petriu, and A. Cordeiro. Human action recognition from local part model. In *Proc. IEEE Int Haptic Audio Visual Environments and Games (HAVE) Workshop*, pages 35–38, 2011. 3
- [17] K. Soomro, A. R. Zamir, and M. Shah. Ucf101: A dataset of 101 human actions classes from videos in the wild. Technical Report CRCV-TR-12-01, CRCV, University of Central Florida, 2012. 4, 6
- [18] C. Sun and R. Nevatia. Large-scale web video event classification by use of fisher vectors. In *Applications of Computer Vision (WACV), 2013 IEEE Workshop on*, pages 15–22. IEEE, 2013. 3
- [19] C. Thureau and V. Hlaváč. Pose primitive based human action recognition in videos or still images. In *Computer Vision and Pattern Recognition, 2008. CVPR 2008. IEEE Conference on*. IEEE, 2008. 3
- [20] A. Vedaldi and B. Fulkerson. VLFeat: An open and portable library of computer vision algorithms. <http://www.vlfeat.org/>, 2008. 7
- [21] H. Wang, A. Kläser, C. Schmid, and C.-L. Liu. Action recognition by dense trajectories. In *CVPR*, pages 3169–3176, 2011. 1
- [22] H. Wang and C. Schmid. Action recognition with improved trajectories. In *International Conference on Computer Vision*, 2013. 1, 3, 6, 7
- [23] H. Wang, M. M. Ullah, A. Kläser, I. Laptev, and C. Schmid. Evaluation of local spatio-temporal features for action recognition. In *BMVC*, pages 127–137, 2009. 5
- [24] C. Yeo, P. Ahammad, K. Ramchandran, and S. S. Sastry. Compressed domain real-time action recognition. In *Multimedia Signal Processing, 2006 IEEE 8th Workshop on*, pages 33–36. IEEE, 2006. 7
- [25] C. Zach, T. Pock, and H. Bischof. A duality based approach for realtime tv-l1 optical flow. In *Ann. Symp. German Association Pattern Recognition*, pages 214–223, 2007. 6
- [26] J. Zhu, B. Wang, X. Yang, W. Zhang, and Z. Tu. Action recognition with actons. *ICCV*, 2013. 1